ACS OMEGA

Open Access

http://pubs.acs.org/journal/acsodf

Article

Novel Deliberately Sensitive and Selective Tetrahydrozoline Voltammetric Sensors Integrated with a Copper Oxide Nanoparticle/Zeolite Platform

Hana M. Abumelha, Ali Sayqal, Razan M. Snari, Kholood M. Alkhamis, Arwa Alharbi, Zehbah A. Al-Ahmed, and Nashwa M. El-Metwaly*

Cite This: *ACS Omega* 2024, 9, 13458−13468

Read Online

ACCESS | Metrics & More | Article Recommendations | Supporting Information

ABSTRACT: The present study introduced a novel disposable screen-printed carbon electrodes (SPCEs) modified with copper oxide/zeolite nanostructures for eco-friendly selective differential pulse voltammetric quantification of tetrahydrozoline (THZ) in eyedrop samples and biological fluids. Modification of the electrode matrix with copper oxide nanoparticles/zeolite nanostructures (CuONPs/ZY) with their effective and synergistic electrocatalytic activity enhanced the electrode performance against electrooxidation of THZ at 0.960 V in BR at pH 9.0 with a diffusion-controlled reaction mechanism. The tentative oxidation mechanism based on molecular orbital calculations postulates the oxidation of THZ molecules through oxidation of a nitrogen atom five-membered ring and the participation of two electrons/protons in the electrode reaction. Linear calibration curves were illustrated within a wide THZ concentration range from 0.24 to 57.2 μg mL^{-1} recording a limit of detection (LOD) value of 0.0799 μg mL^{-1}. The CuONPs/ZY/SPEs exhibited improved performance compared with the sole reported THZ sensor-based gold film-plated carbon paste electrodes, in addition to their high reproducibility of fabrication and measurement and prolonged shelf lifetime. Tetrahydrozoline was successfully assayed in the presence of excipients, degradation products, and chloramphenicol. The presented voltammetric sensor can be considered as an eco-friendly and reliable analytical approach for monitoring THZ residues in eye drop samples and biological fluids with high recovery compared with the official pharmacopeial analytical protocol. The presented sensors were assessed according to an EcoScale tool and also compared with the reported THZ sensor.

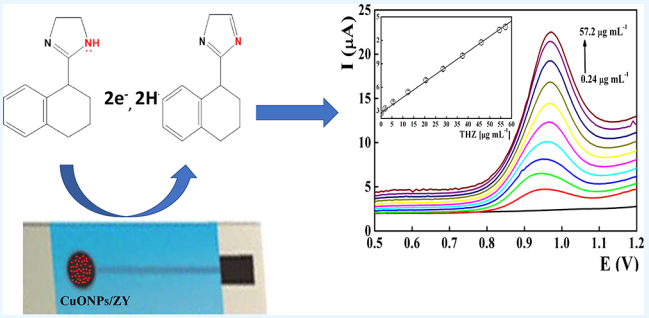

1. INTRODUCTION

Tetrahydrozoline (THZ; 1*H*-imidazole, 4,5-dihydro-2-(1,2,3,4-tetrahydro-1-naphthalenyl) hydrochloride), is an active ingredient in pharmaceutical ophthalmic solutions of nasal sprays and eye drops to treat conjunctivitis and rhinitis as a nasal or ocular decongestant.[1−3] THZ is a selective α_1-receptor agonist that belongs to the sympathomimetic family, causing local vasoconstriction in the eye to enhance nasal congestion, ocular irritation, and allergic rhinitis.[3−5] Its effects cross the blood−brain barrier on the α_2-receptor were explained to diminish the central sympathetic outflow, which causes parasympathetic activity (bradycardia and hypotension).[6−8]

THZ absorbs rapidly after its topical administration, and it is safe when applied topically on nasal/ocular tissue. On the other hand, THZ rapidly crosses the blood−brain barrier if it is given parentally or enterally to work against α_2-adrenoceptors to inhibit the sympathetic vasomotor centers and reduce the peripheral vascular tone. Other THZ side effects may include miosis, dry mouth, hypotension, respiratory depression, bradycardia, sedation, hypothermia, and hyporeflexia.[3,7−11] In children, accidental oral ingestion results in profound sedation, hypotension, shock, and possibly profuse sweating.[3,6,12]

Recently, THZ has gained legal attention due to its abuse for criminal and nefarious nonmedicinal purposes such as drug-facilitated sexual assault (DFSA) and homicide.[13−15] Studies have shown that THZ concentration values higher than the upper normal limit values (13−210 ng mL^{-1} in blood or 11−40 ng mL^{-1} in urine) advocated the nonmedicinal uses of the drug.[16] THZ is not a routinely suspected drug that is commonly used in criminal activity, especially in standard drug analysis screens, since its characteristics make it go unnoticed. THZ's effect is so powerful; even a very small quantity administered orally can result in many serious clinical

Received: January 11, 2024
Revised: February 28, 2024
Accepted: March 1, 2024
Published: March 8, 2024

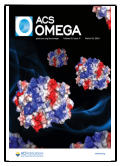

effects.[5,6,9] Moreover, monitoring low concentration levels of THZ in biological fluids is a crucial issue in determining the overdose if accidently ingested by children.[16] However, rapid diagnostic tools for monitoring THZ residues in treatment modalities and biological fluids for its toxicity are scarce.

Determining a drug's safety and efficacy profile needs analytical tools that are able to simultaneously detect the target analyte in a mixture of interfering substances and degradation products and to determine drug residues in various biological conditions. UV spectrophotometry and nonaqueous potentiometric titration were the official pharmacopeial methods for THZ.[17,18] Chromatographic approaches including HPLC,[19−21] RP-HPLC,[22,23] HPTLC densitometric method,[24] and capillary electrophoretic[25] methods were the most common techniques. Although hyphenated chromatographic instrumentations provide accurate quantification of pharmaceutical products in biological samples, they are expensive and complex and require separate analysis for each drug. Moreover, UV[19,26−28] and colorimetric charge transfer complex formation with TCNQ and TCNE reagents were also reported[29] with various sensitivities for monitoring of THZ's pharmaceutical formulations.

The commonly used chromatographic/spectrophotometric methods come with complexities in preparation, operation, and maintenance, involving large production of toxic waste solvents having low sensitivity, which hinder their applicability for medical and forensic purposes. Current advancements are being oriented toward electrochemical sensors as a promising tool for monitoring of pharmaceutical residues. Electroanalytical approaches are considered as simple, quick, and low-cost analysis protocol.[30−33] In this regard, PVC membrane selective potentiometric sensors based on THZ ion associates with tetraphenyl borate, phosphomolybdic acid, and phosphotungstic acid were constructed for monitoring of THZ in ophthalmic solution and biological samples.[34] More recently, screen-printed potentiometric electrodes integrated with β-cyclodextrin or calixarene as molecular recognition elements were reported for simple potentiometric determination of THZ in eye drop preparations and rabbit tears.[35] To the best of our knowledge, only gold film-plated carbon paste electrodes (Au/CPEs) were presented for differential pulse voltammetric determination of THZ eye drops from and urine samples.[36] The cited electrodes showed linear working concentrations ranging from 1.99×10^{-5} to 7.79×10^{-5} mol L^{-1} and an LOD value of 5.54×10^{-6} mol L^{-1}.

Electrochemical methods based on screen-printed electrodes (SPEs) have been emerging as promising candidates for healthcare monitoring and commercialization of electrochemical sensors.[37−41] Screen printing technology offers mass production of disposable devices that integrate the working, reference, and auxiliary electrodes on a compact substrate. Recent research has been devoted to integration of electrochemical sensors with various nanostructures to enhance the sensing performance such as their selectivity, sensitivity, and response time. Several trials were performed to incorporate different metallic oxide nanostructures within the electrochemical sensor matrix.[41−51] As a common metallic oxide nanostructure, copper oxide nanoparticles (CuONPs) were utilized as a proper electrode modifier for electrochemical sensing of many pharmaceutically active compounds.[52−56] Zeolitic nanostructures showed promising characteristics such as shape, pore size, and high cation exchange capacity; therefore, they were reported as a recommended modifier for various electrochemical sensors in determining many biologically and pharmaceutically active compounds.[57−60]

In the present study, the research team developed and validated a screen-printed sensor based on zeolite and copper nanoparticles for the selective determination of THZ in biological and eye drop samples in the coexistence of different THZ degradation products and other expected interferants. The sensor demonstrated high sensitivity, selectivity, accuracy, and precision as well as a simple, rapid, and eco-friendly fabrication and analysis procedure. We propose this electrochemical sensor as a potential tool for both the quality control and therapeutic monitoring of THZ.

2. EXPERIMENTAL SECTION

2.1. THZ Sample and Chemicals. A tetrahydrozoline hydrochloride authentic sample (THZ, $C_{13}H_{17}ClN_2$, 236.74 g mol^{-1}, purity 100.80 ± 0.92) was supplied by Sigma-Aldrich (CAS Number 522-48-5). The fresh THZ solution was prepared on a daily basis by dissolving the authentic THZ sample in deionized water. The disposable screen-printed carbon working electrodes were constructed as described in detail elsewhere[61] using the commercial printing carbon ink (Electrodag 421 SS, Acheson, UK). Different metallic oxide nanopowders were tested as electrode modifiers including copper oxide (<50 nm particle, 544868 Sigma-Aldrich), iron oxide (Sigma-Aldrich), and zinc oxide (Sigma-Aldrich) in addition to Zeolite Y (NISTRM8850, Sigma-Aldrich). The standard drug-free biological samples were purchased from VACSERA (Giza, Egypt). Universal buffer (4.0×10^{-2} mol L^{-1}) was prepared by mixing a calculated amount of boric acid, phosphoric acid, and acetic acid in bidistilled water, and the required pH value was adjusted with NaOH.

2.2. THZ Pharmaceutical and Biological Samples. The THZ hydrochloride pharmaceutical samples (VISINE Eye Drops 0.05% THZ, Pfizer, Egypt) were obtained from local markets. After suitable dilution with water, samples were transferred to the measuring cell and assayed voltammetrically compared with the pharmacopoeial method.[18]

A plasma sample was fortified with known aliquots of the THZ standard solution and mixed with acetonitrile (1:3 ratio) to remove the residual protein, and the volume was adjusted to 10 mL with water. Aliquots of the treated sample were transferred to a voltammetric cell containing 15 mL of the BR buffer at pH 9, where the THZ residue was monitored voltammetrically, as described earlier. Urine samples were mixed with different aliquots of the THZ authentic sample. The pH of the sample was adjusted to pH 9, and the THZ content was assayed voltammetrically, following the pharmacopeial recommendations.

2.3. Forced Degradation Studies. The THZ forced degradation protocols were performed under acidic, alkaline, oxidative, or thermal stress conditions or photolytic degradation.[25] The standard THZ solutions were separately treated with 1.0×10^{-1} mol L^{-1} HCl, NaOH, or 3% H_2O_2 for the acidic, alkaline, or oxidative degradation process, respectively. The UV stability included exposure of the solid THZ powder under UV light at 254 nm for 24 h, and thermal degradation was realized in an oven at 100 °C for 24 h. The residual undegraded THZ was assayed under pharmacopeial and voltammetric analysis protocol.

2.4. Copper Oxide/Zeolite-Based Printed Sensors and Measuring System. Cyclic, differential pulse voltammetric, and chronoamperometric measurements were carried out using

https://doi.org/10.1021/acsomega.4c00370
ACS Omega 2024, 9, 13458−13468

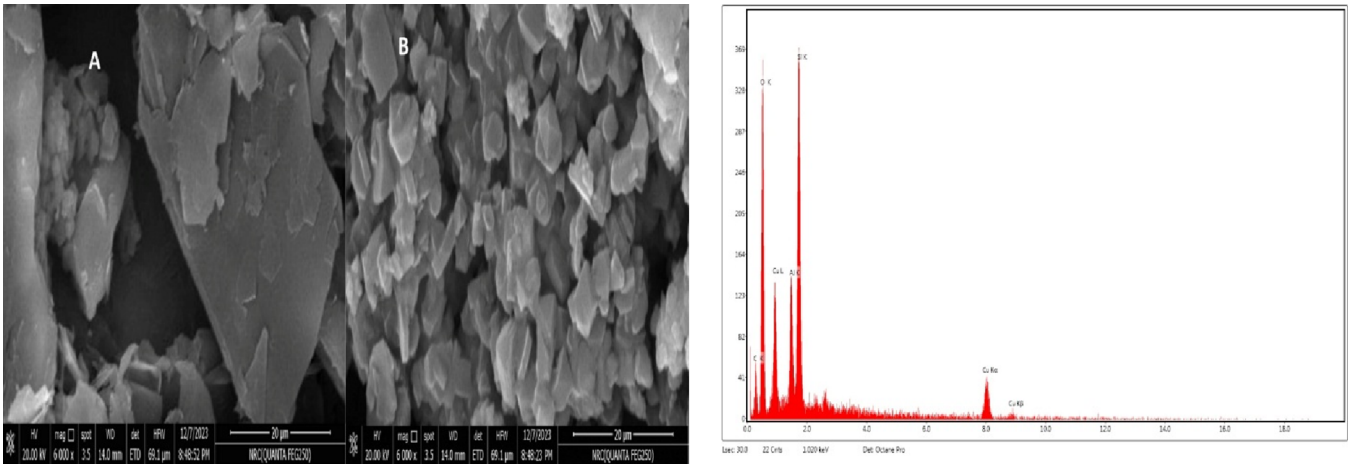

Figure 1. SEM images and EDX of the CuONP/ZY-integrated screen-printed sensors.

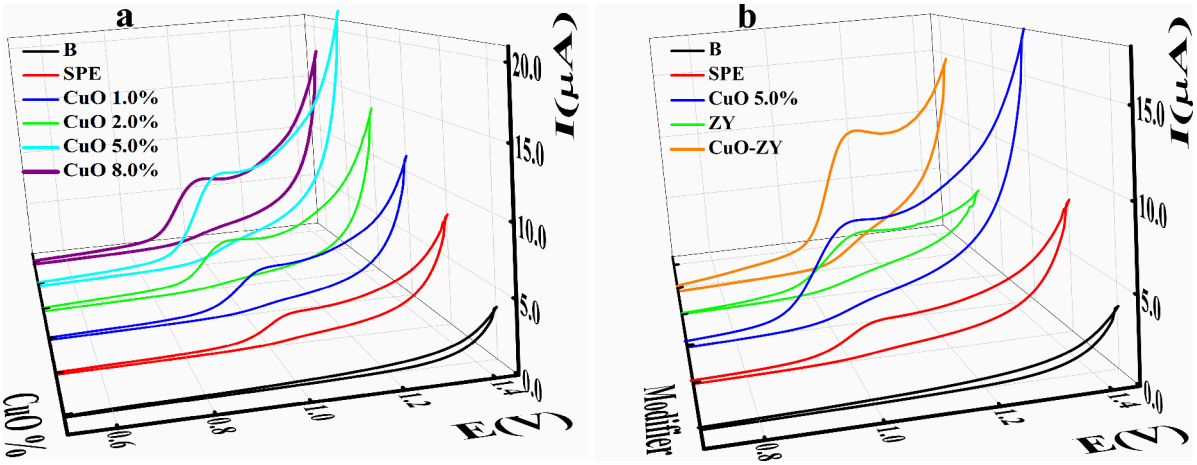

Figure 2. (a) Cyclic voltammograms recorded for 20 μg mL^{-1} THZ at sensors integrated with different CuONPs ratios. (b) Performance of sensors integrated with CuONPs and ZY nanostructures. The applied scan rate was 60 mV s^{-1} at pH 9.0.

a Metrohm workstation (797 VA Metrohm, Switzerland) in a three-electrode thermostated cell (25 ± 1.0 °C) containing a platinum wire auxiliary electrode and a silver/silver chloride reference electrode, in combination with the integrated printed carbon sensors as working electrodes. Copper oxide/zeolite fortified ink (composed of 10 mg of CuONPs, 10 mg of ZY, and 180 mg of the commercial carbon ink) was printed onto the PVC sheet through a stainless-steel mesh.[61] After curing at 50 °C for 60 min, the printed sensors were segmented into individual sensor strips and covered with an insulator layer with a working circular area of 3 mm.

Chronoamperometric measurements were performed in the thermostated cell containing 15 mL of BR buffer (pH, 9 0) under continuous stirring. The cell potential was fixed at 0.960 V, and after the achievement of a stable baseline, known aliquots of the standard authentic THZ solution were spiked to the electrochemical system and the current values were monitored.

2.5. Recommended Analysis Protocol. A thermostated measuring cell containing 15 mL of BR buffer at pH 9 was fortified with known ascending increments of the standard THZ authentic solution. After each addition, the DPVs were monitored at the following optimized electroanalytical measuring parameters: pulse amplitude 50 mV; pulse width 100 ms; pulse duration 40 ms; scan rate 60 mV s^{-1}; voltage step 6 mV; and voltage step time 0.15 s.

2.6. Oxidation Mechanism and Molecular Orbital Calculations. The tentative oxidation mechanism of the THZ molecule at the CuONP/ZY-fortified printed sensors was studied based on molecular orbital calculations (MOC) utilizing the MP7 model through MOPAC software.[62]

3. RESULTS AND DISCUSSION

3.1. Morphological Characterization of the CuONP/ZY-Integrated Screen-Printed Carbon Sensors. The surface morphology of the fabricated sensors integrated with copper oxide/zeolite nanoparticles was examined using scanning electron microscopy (SEM) compared with the bare electrode surface (Figure 1a,b). Following the in situ incorporation of CuONPs, the SEM images revealed the emergence of bright points, indicating the presence of clusters of copper on the electrode surface. These bright points likely signify the formation of copper-based structures as a result of the modification process. The observed clusters contribute to the overall understanding of the morphological changes induced by the introduction of CuONPs. Additionally, the SEM analysis exhibited distinct features related to the zeolite Y modification. Characteristic flake-shaped particles were identified, providing visual evidence of the presence and arrange-

https://doi.org/10.1021/acsomega.4c00370
ACS Omega 2024, 9, 13458−13468

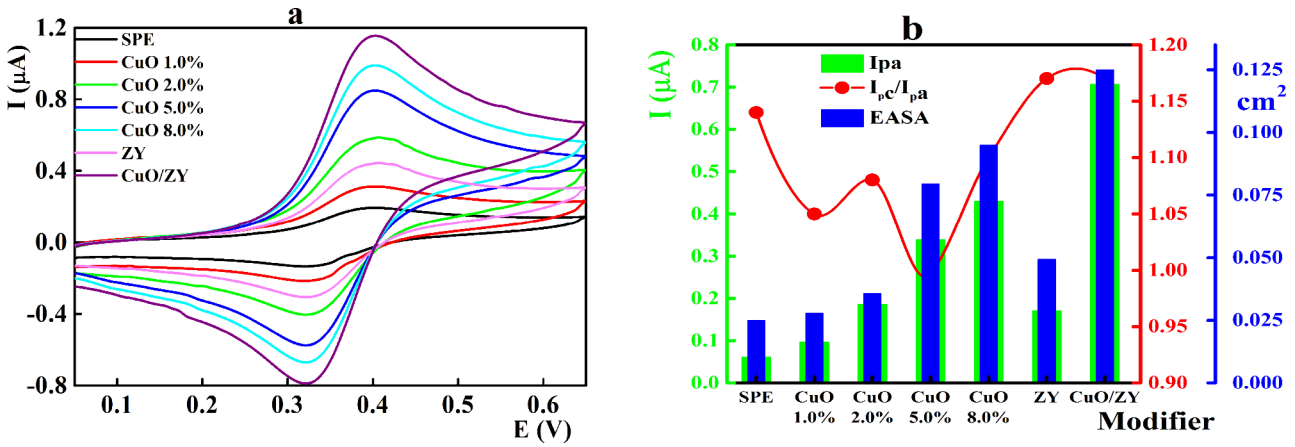

Figure 3. (a) CVs recorded in 5.0×10^{-3} mol L^{-1} $[Fe(CN)_6]^{3-/4-}$ solution at CuONPs/ZY/SPCEs. (b) The estimated peak current and electroactive surface area for the CuONPs/ZY/SPCEs.

Table 1. Redox Characteristic Peak and Electroactive Surface Area for the CuONPs/ZY/SPEs

electrode	E_{pa} (V)	E_{pc} (V)	ΔE (V)	I_{pa} (μA)	I_{pc} (A)	$I_{pc/Ipa}$ (A)	active area (cm^2) ± SE[a]
SPE	0.401	0.33	0.071	0.0608	−0.0694	1.14	0.0250 ± 0.002
CuO 1.0%	0.401	0.33	0.071	0.0973	−0.1020	1.05	0.0280 ± 0.003
CuO 2.0%	0.395	0.324	0.071	0.1860	−0.2000	1.08	0.0358 ± 0.003
CuO 5.0%	0.395	0.318	0.077	0.339	−0.3380	0.997	0.0795 ± 0.006
CuO 8.0%	0.407	0.33	0.077	0.4300	−0.4750	1.10	0.0950 ± 0.005
ZY 5.0%	0.395	0.33	0.065	0.171	−0.2000	1.17	0.0495 ± 0.003
CuO/ZY	0.395	0.324	0.071	0.7070	−0.8250	1.17	0.1250 ± 0.007

[a]SE for three tropical measurements.

ment of a zeolite Y nanostructure at the electrode surface. Furthermore, porous conglomerates of compact crystals were observed, suggesting a unique structural arrangement resulting from the application of the zeolite Y nanostructure.

Confirmation of the electrode matrix modifications was corroborated through energy-dispersive X-ray (EDX) analysis with unveiled detectable quantities of copper oxide and zeolite Y nanoparticles at the printed electrode surface (Figure 1b).

3.2. Electrochemical Oxidation of THZ at CuO-ZY-Integrated Sensors. At the Au/CPEs, THZ showed an irreversible anodic oxidation peak at 0.915 V in the presence of a suitable surface-active agent with at pH 10.[36] Based on the electrocatalytic effect of different metallic oxide nanostructures, homemade-printed sensors integrated with copper oxide/zeolite nanostructures were introduced for sensitive voltammetric determination of THZ. At the unmodified electrode surface, THZ exhibited a low current broad anodic oxidation peak at 1.05 V due to the slow electron transfer process at the bare electrode surface (Figure 2a). Upon fortification of the printing ink with CuONPs, the THZ oxidation peak was amplified and shifted toward the cathodic direction due to the electrocatalytic effect of CuONPs. This electrocatalytic effect may be attributed to the presence of Cu (III)/Cu (II) redox transitions, which are able to oxidize the THZ molecule at the electrode surface.[53,63] The estimated results indicated duplication of the THZ peak current via incorporation of 1.0% CuONPs within the electrode matrix. Gradual enhancement of the peak performance was recorded at a higher modifier content to reach its maximum peak current at 5.0% CuONPs. No significant improvement of the electrode performance was recorded at a higher content of CuONPs, and therefore, 5.0% CuONPs were selected for further investigation. Next, CuONPs were replaced with the same amounts of other metallic oxide nanostructures to select the most proper one (Figure S1). Among the tested oxides, CuONPs were the most proper, which may be explained on the basis of the oxidation potential and the band gap of the oxide forms.

Zeolitic nanostructures possess excellent characteristics as electrode modifiers based on their configurations, structures, pore size, and high cation exchange capacity. Therefore, the present study was oriented to introduce the zeolitic structure in combination with CuONPs as an electrode modifier (Figure 2b). At the working electrodes modified with ZY, THZ showed an oxidation peak at 1.1 V with an improved peak current compared with the bare electrode. Sensors fortified with CuONPs/ZY composites showed enhanced peak currents compared with all previous studied electrodes, which can be explained by the synergistic electrocatalytic effect of both modifiers and the enhanced electroactive surface area upon modification with CuONPs/ZY nanocomposites.

To confirm the impact of the electrode modification on the electrochemical behavior of the CuONP/zeolite-integrated sensors, cyclic voltammograms were monitored in a ferricyanide (FCN) solution. A gradual increase of the anodic and cathodic peak currents was recorded upon modification of the electrode matrix based on enhancement of the electroactive surface area and acceleration of the electron transfer process at the electrode surface (Figure 3 and Table 1). For example, the recorded anodic peak current increased from 0.0608 μA at the bare electrode to 0.339 μA for 5.0% copper oxide integrated sensors and to 0.707 μA for the CuONP/ZY-based sensors.

Next, the estimated electroactive surface area for sensors modified with different copper oxide and zeolite ratios was

https://doi.org/10.1021/acsomega.4c00370
ACS Omega 2024, 9, 13458−13468

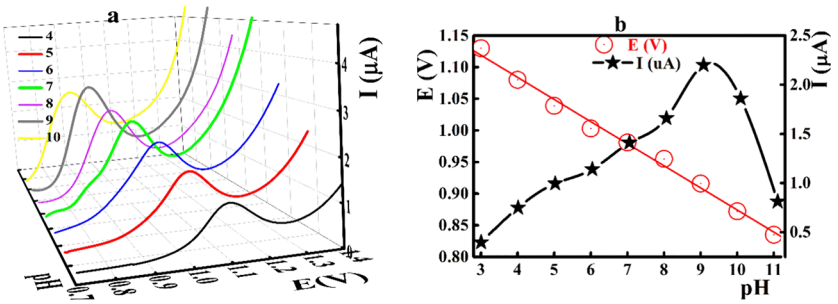

Figure 4. (a) Differential pulse voltammograms recorded at different pH values in the presence of 2.0 μg mL^{-1} THZ. (b) The oxidation peak potential and current values versus the pH of the supporting at the CuONPs/ZY/SPCEs and a scan rate value of 60 mV s^{-1}.

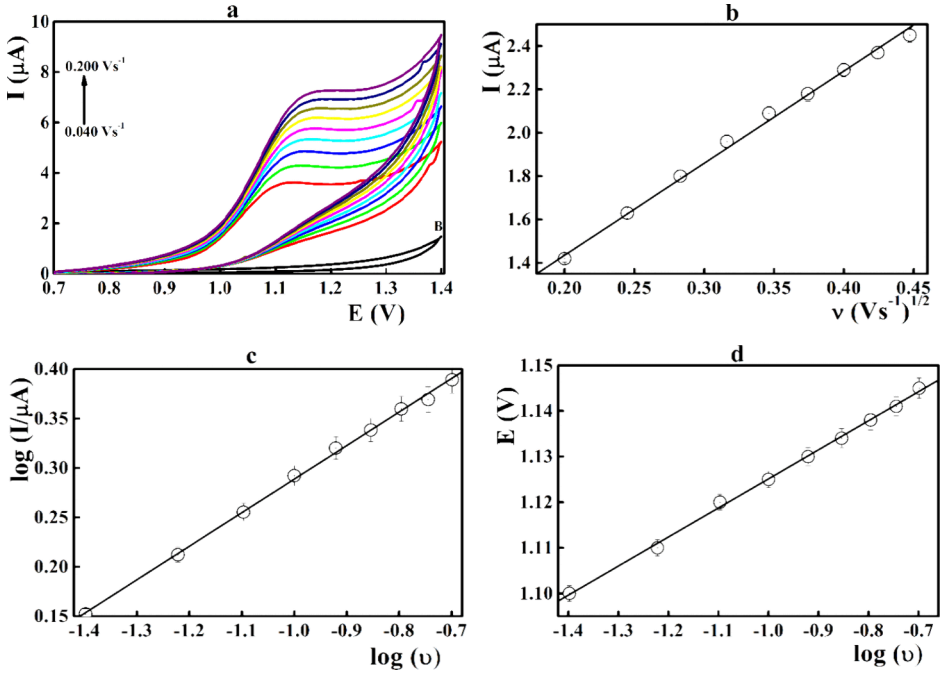

Figure 5. (a) Cyclic voltammograms recorded at different scan rate values in the presence of 4.0 μg mL^{-1} THZ. (b) The estimated peak current versus the square root of the scan rate values. (c) Relation of the logarithmic values of the peak current against logarithmic values of the scan rate. (d) Peak potential against the logarithmic value of the applied scan rate. Average of three experiments.

calculated by recording successive cyclic voltammograms at different scan rate values in the FCN solution. At each applied scan rate, the anodic peak current was plotted against the square root value of the corresponding scan rate where the electroactive surface area was calculated based on the Randles−Sevik equation.[64] The estimated electroactive surface area increased from 0.025 cm^2 for bare screen-printed sensors to 0.095 and 0.125 cm^2 for the 5.0% CuONP- and CuONP/ZY-based sensors, respectively. Furthermore, the active surface area of the carbon screen-printed electrode, modified with CuONPs, surpassed the geometric area of the electrode. This alignment between the higher active area and the results derived from both the morphological images and EDX analysis reinforces the accuracy and consistency of the obtained findings.

3.3. Voltammetric Behavior of THZ at Different pH Values. THZ showed a pK_a value of 10.5[65]; therefore, it is expected that the electrochemical behavior of the THZ molecule at the CuONP/ZY electrode surface is pH-dependent. As illustrated in Figure 4a, the oxidation potential of the recorded differential pulse voltammograms was shifted to more negative values at evaluated pH levels, assuming the participation of the protons in the electrooxidation of the THZ molecule.[66−68] Plotting the recorded peak potential versus the pH values revealed a linear relationship with a near Nernstian slope value [$E_{(V)}$ = 1.2238−0.0425 ± 0.0012 [pH], r = −0.9963, Figure 4b]. The slope value postulates participation of an equal number of electrons/protons in the electrode reaction, and the small intercept value indicated the absence of side electrode reaction, which agreed with the previous report for THZ at the gold film-plated carbon paste electrode.[36]

The recorded peak height gradually increased to reach its maximum value at pH 9 (near the pK_a value of THZ), which is selected for the next measurements.

3.4. Voltammetric Behavior of THZ at Different Sweep Rates. Recording the cyclic voltammograms at different scan rates can explore the electrode reaction mechanism and estimate the number of electrons, which involves electrooxidation of the THZ molecule at the CuONP/ZY/SPCE electrode surface.[66] As illustrated in Figure 5a, the THZ molecule showed an irreversible single anodic oxidation peak, which enhanced the peak current values at a higher scan rate with continuous shifting of the peak potential toward the anodic direction.

https://doi.org/10.1021/acsomega.4c00370
ACS Omega 2024, 9, 13458−13468

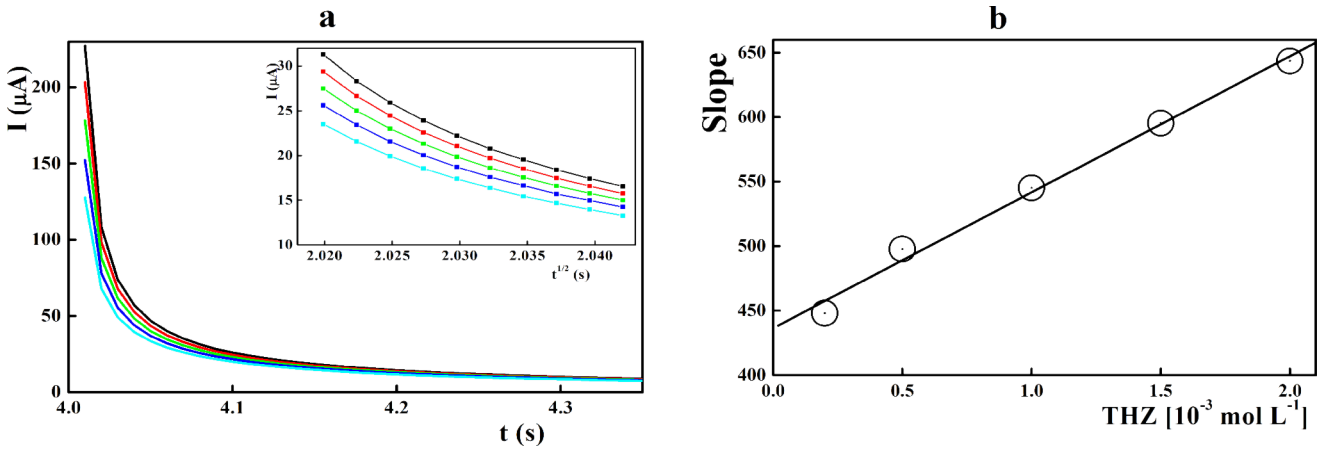

Figure 6. (a) Chronoamperograms recorded at the CuONP/ZY/SPCE surface (pH 9.0) in the presence of different THZ concentrations; the inset figure represents the value of current against $t^{-1/2}$ estimated from chronoamperograms and (b) slope values against the THZ concentration.

A linear relationship (r = 0.9986, Figure 5b) correlates the recorded peak current values with the square root value of the scan rate, which assumes the irreversibility of the electrode reaction. The logarithmic values of the peak current showed a linear relationship against the logarithm value of the scan rates [log I (μA) = 0.6282 + 0.3394 ± 0.0049 [log (υ/V s^{-1})], r = 0.9993; Figure 5c], where the slope value 0.3394 μA V s^{-1} postulated a diffusion-controlled electrode reaction.[66−68] This electrode reaction mechanism disagrees with those described in the case of a gold-plated carbon paste electrode, which indicated an adsorption reaction mechanism with a linear slope value of 0.722.[36]

Figure 5d illustrates the correlation between the peak potential ($E_{(V)}$) for oxidation of the THZ molecule and the logarithmic value of the applied scan rate (ν). The observed linear relationship is expressed by the equation $E_{(V)}$ = 1.1888 + 0.0537 ± 0.0010 [log υ], r = 0.9991. At higher scan rates, the peak potential becomes more negative, suggesting that the electrochemical reaction follows a standard irreversible process according to the Laviron equation.[69]

$$E_p = E^0 + \left(\frac{2.303RT}{\alpha nF}\right)\log\left(\frac{RTK^0}{\alpha nF}\right) + \frac{2.303RT}{\alpha nF}\log u$$

Here, R is the ideal gas constant (8.314 J/K mol), n represents the total number of electrons transferred, α is the electron transfer coefficient, F is the Faraday constant (96,480 C/mol), and T is the temperature (298 K). By evaluating the slope of E_p and log ν 0.0537, the product of αn is calculated as 1.115. Subsequently, α is determined using the formula

$$\alpha = \frac{47.7}{E_p - E_{1/2}}$$

$E_{1/2}$ (mV) is the potential at which the current is at half the peak value, which was estimated using EC-Lab V10.40 software (Figure S2). The calculated α is found to be 0.7338, leading to an approximate value of 1.52 ($n \approx 2$) compared to one electron for the previous carbon paste electrode.[36] This result indicates that two electrons are involved in the electrochemical process of THZ. Next, the apparent heterogeneous electron transfer rate constant (κ_s) is determined using the following equation[70]:

$$\kappa_s = \alpha nF\nu/RT$$

where ν represents the selected scan rate, set at 0.05 V/s. The final calculation yields the κ_s value as 2.1712 s^{-1}.

To monitor the chronoamperometric measurements of THZ at the CuONP/ZY/SPCE surface, the electrode potential was stabilized at the THZ oxidation potential (0.960 V) in the presence of various THZ concentrations at pH 9.0 (Figure 6). The corresponding current for each THZ concentration was measured against time, as illustrated in Figure 6. The diffusion coefficient at the mass transport limited rate was calculated based on the Cottrell equation.[66]

$$I = nFAD^{1/2}C_b\pi^{-1/2}t^{-1/2}$$

where C_b is the bulk concentration of THZ and D is the diffusion coefficient of THZ.

The recorded current values were plotted versus the $t^{1/2}$ at different THZ concentrations (Figure 6a inset), where the slope value was plotted against the THZ concentrations (Figure 6b) where the slope value represents the diffusion coefficient, which is equal to 3.6 × 10^{-5} cm^2/s.

The development of a voltammetric oxidation mechanism of the THZ molecule at the CuONP/ZY/SPCE surface involves a comprehensive approach that integrates experimental results with MOC utilizing the MP7 model through MOPAC software.[62] The proposed tentative oxidation mechanism of the THZ molecule is outlined in Scheme 1. Through MOC

Scheme 1. Preliminary Oxidation Mechanism of the THZ Molecule at CuONPs/ZY/SPCEs; pH 9.0.

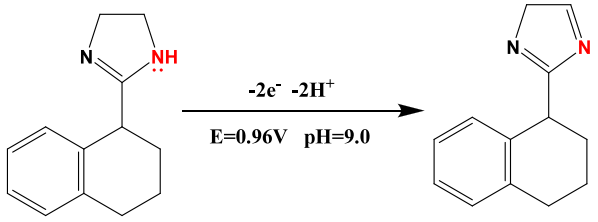

conducted with the MP7 model using MOPAC software (Figure S3 and Table S1), it becomes evident that the nitrogen atom at position 5 within the THZ molecular structure exhibits the highest electron density.[71] Consequently, this nitrogen atom is more prone to the loss of two electrons during voltammetric anodic oxidation, occurring at a potential of

https://doi.org/10.1021/acsomega.4c00370
ACS Omega 2024, 9, 13458−13468

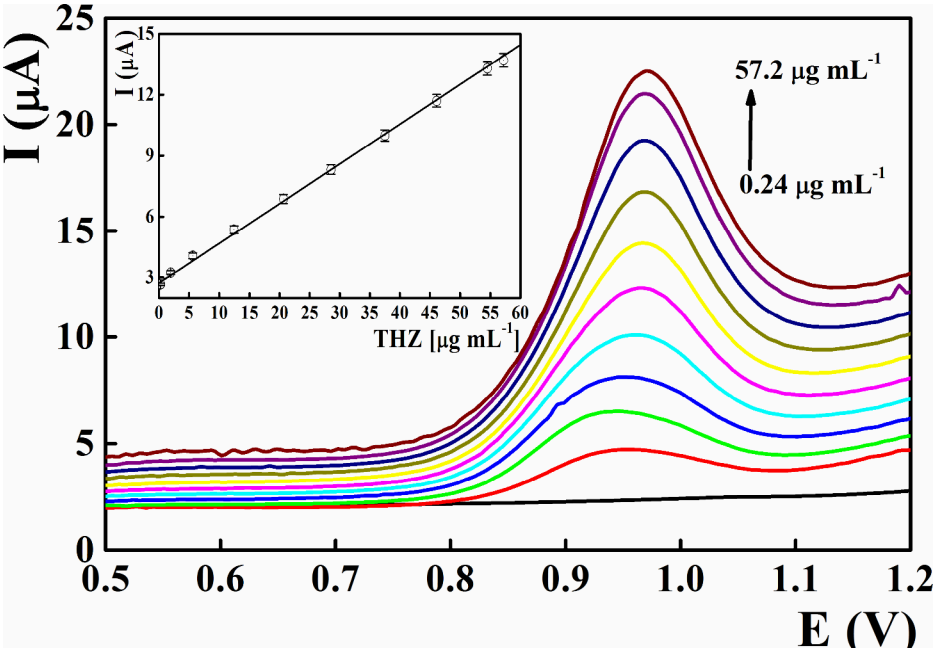

Figure 7. Differential pulse voltammetric determination of tetrahydrozoline in CuONP/ZY nanostructure-integrated screen-printed sensors at pH 9. Average of five experiments.

0.960 V. This mechanism agreed with that reported on the gold-plated carbon paste electrode.[36]

3.5. Validation of the CuONPs/ZY/SPCEs. The electroanalytical features of the constructed THZ disposable sensors integrated with the CuONP/ZY nanostructure were validated applying the optimized electroanalytical parameters (Figure 7 and Table 2). Ascending aliquot concentrations of the authentic standard THZ solution were added to the supporting electrolyte at pH 9.0, and the peak currents of the monitored DPVs were plotted against the THZ concentration. Linear calibration graphs (r^2 = 0.9993) were constructed covering a wide THZ concentration range from 0.24 to 57.2 μg mL^{-1}. Based on the slope and standard deviation values of the linear curve, the recorded values of limit of quantification (LOQ) and limit of detection (LOD) were 0.2422 and 0.0799 μg mL^{-1}, respectively.[72]

Table 2. Performance and Electroanalytical Features of the Copper Oxide/Zeolite Nanostructure-Based Screen-Printed Sensors

parameters	value[a]
selected pH value	9.0
oxidation potential (V)	0.960
linearity range (μg mL^{-1})	0.24−57.2
slope (μA mL^{-1} μg^{-1})	0.1907
intercept (μA cm^{-2})	2.8766
SD_{slope} (μA mL^{-1} μg^{-1})	0.0018
$SD_{intercept}$ (μA cm^{-2})	0.0046
r^2	0.9993
RSD %	0.1168
LOD (μg mL^{-1})	0.0799
LOQ (μg mL^{-1})	0.2422
repeatability of the peak current (RSD %)	1.35
reproducibility of the peak current (RSD %)	0.84
reproducibility of the peak potential (RSD %)	1.22
repeatability of the peak potential (RSD %)	0.95

[a]Average of five experiments.

The sole reported THZ voltammetric sensor based on a gold-plated carbon paste electrode showed a linear working range from 1.99 × 10^{-5} to 7.79 × 10^{-5} mol L^{-1} with LOQ and LOD values of 1.69 × 10^{-5} and 5.54 × 10^{-6} mol L^{-1}, respectively.[36] Compared with sensitivity values reported for the CuONPs/ZY/SPCEs (Table S2), the presented disposable sensors showed improved sensitivity (about 1.68 × 10^4 fold) with the advantage of having a planar design suitable for small-volume measurements and decentralization measurements. The repeatability of the peak current was evaluated by running seven successive DPVs for 30 μg mL^{-1} of the THZ authentic solution with the same printed electrode surface. High repeatability of the peak current (RSD% = 1.35) was reported. The fabrication reproducibility was performed by testing seven printed sensors within the same batch under the same experimental conditions, and the recorded RSD value for the aforementioned THZ concentration was 3.65%. The shelf lifetime of the printed sensors was monitored over a prolonged storage period of up to 6 months, and the measured peak current values were stable and reproducible.

3.6. Selectivity. For registration of a new pharmaceutical compound for human consumption, the International Conference on Harmonization (ICH) recommended technical requirements for further studies on impurities such as degradation products and reaction residues of the drug substance and excipient.[73,74] Impurities present in the final formulation should preferably be identified and/or quantified. Moreover, some of these impurities have similar chemical structures to the parent drug.

The selectivity of the presented CuONPs/ZY/SPCEs was demonstrated by monitoring the forced degradation behavior of THZ under stress conditions (acid and base hydrolysis and oxidative). The THZ molecule is stable under oxidative degradation conditions, exposure to UV light, under heating conditions.[25] Less stability was recorded under basic and acidic

https://doi.org/10.1021/acsomega.4c00370
ACS Omega 2024, 9, 13458−13468

Table 3. Analysis of Tetrahydrozoline in Eye Drop Solution and Biological Fluids

sample	taken (μg mL^{-1})	found* (μg mL^{-1})	bias%	recovery (%)	pharmacopoeia [18]
VISINE	5	5.03	0.50	100.50	100.80
	15	14.95	0.33	99.67	100.20
	30	30.07	0.23	100.23	99.40
	50	50.30	0.60	100.60	99.70
mean				100.25	100.03
variance				0.18	0.38
observations				4	4
df				3	3
t-test	0.61				
F	2.14				
t critical two-tail	2.45				
sample	**add (μg mL^{-1})**	**found* (μg mL^{-1})**	**bias%**	**recovery (%)**	**pharmacopoeia [18]**
spiked urine	10	10.05	0.50	100.50	100.70
	20	20.12	0.33	100.60	99.40
	40	39.70	0.23	99.25	100.10
mean				100.12	100.07
variance				0.57	0.42
observations				3	3
df				2	2
t-test	0.17				
F	1.33				
t critical two-tail	2.78				
F critical one-tail	19.00				
sample	**added (ng mL^{-1})**	**found (ng mL^{-1})**	**recovery (%)**	**SD**	**% RSD**
plasma	100	100.5	100.50	0.120	1.34
	220	218	99.09	0.085	1.22
	350	352	100.57	0.055	0.95

*Average of five replicates measurement

conditions where 10.2 and 4.3%, of the original THZ degraded under basic and acidic conditions, respectively. When subjected to alkali degradation, THZ produces *N*-(2-aminoethyl)-1,2,3,4-tetrahydro-1-naphthamide.[34,75,76] The formed degradation product did not show noticeable interference or overlap with the main THZ oxidation peak at 0.960 V.

Different excipients and additives are usually present in the final pharmaceutical formulation. These species may cause serious interference during assaying of the active pharmaceutical compound and result in false information about the content of the target analyte; therefore, monitoring the interference of such species is a quite crucial issue for modern drug quality control. In the present study, the interference of common additives such as starch, citric acid, glucose, propylene glycol, metal ions, and preservatives was investigated. High tolerance limits were reported with acceptable recovery values in the presence of excipients and preservatives.

Moreover, the simultaneous voltammetric measurement of both THZ and chloramphenicol (CAP), which is usually present in eye drop pharmaceutical formulations, was studied. At the CuONPs/ZY/SPCEs, well-defined and separated oxidation peaks were recorded for CAP and THZ at 0.255 and 0.960 V, respectively, confirming the applicability of the presented analytical approach for simultaneous voltammetric determination of both pharmaceutically active components (Figure S4).

3.7. Analysis of Pharmaceutical and Biological Samples. The fabricated THZ disposable sensors based on the CuONPs/ZY nanostructure offered improved sensitivity and selectivity toward THZ and can be introduced as a suitable analytical tool for sensitive voltammetric determination of THZ in eye drop solution and biological fluids. The tested biological samples were fortified with known ascending aliquots of the authentic THZ solution and assayed according to the presented voltammetric and pharmacopeial recommendation based on nonaqueous potentiometric titration (Table 3). The tabulated data revealed high recovery, which encourages their applicability for mentoring THZ residues in biological and eye drop samples.

3.8. Green Chemistry Assessment. The planar disposable screen print modified with copper oxide/zeolite nanostructures and the proposed electroanalytical approach were involved for an assessment of environmental risks, reliability, and suitability according to a semiquantitative environmental analytical scale.[77,78] This environmental analytical scale is mainly governed by the penalty points based on the chemical hazards, potential exposure, energy consumed during fabrication and measurement, and waste treatment protocol. In the present study, the penalty score (Table S3) for construction of the disposable sensor and analysis protocol was found to be 81 compared with 48 for the gold-plated carbon paste electrode, indicating the suitability and eco-friendliness of the proposed electroanalytical approach.[79]

4. CONCLUSIONS

A novel planar disposable screen-printed carbon sensor modified with copper oxide/zeolite nanostructures was introduced as a reliable and efficient analytical tool for sensitive and selective differential pulse voltammetric quantification of THZ in eye drop samples and biological samples in the coexistence of different excipients, degradation products, and CAP. Copper oxide and zeolite nanostructures exhibited

https://doi.org/10.1021/acsomega.4c00370
ACS Omega 2024, 9, 13458−13468

electrocatalytic activity toward oxidation of THZ at pH 9 with improved sensitivity covering a wide concentration range from 0.24 to 57.2 μg mL^{-1} and an LOD value of 79.9 ng mL^{-1}. The presented sensors were successfully applied for determination of THZ in eye drops and biological fluids with high precision and accuracy. Compared with the previously reported THZ voltammetric sensors, the present sensor showed improved sensitivity with the advantages of mass production and high reproducibility of measurement. Moreover, these presented fabrication protocols are expected to provide new insight into the effective sensing ability of the low-cost electroanalytical approach, which could provide a valuable tool for monitoring of pharmaceutical residues and drug quality control.

■ ASSOCIATED CONTENT

Data Availability Statement

All data generated or analyzed during this study are included in this published article (and the Supporting Information).

Supporting Information

The Supporting Information is available free of charge at https://pubs.acs.org/doi/10.1021/acsomega.4c00370.

Cyclic voltammograms for THZ recorded at screen-printed sensors with different metallic oxide nanostructures; estimation of the E_p and $E_{1/2}$ of the THZ; chemical formula of the tetrahydrozoline molecule; computed molecular orbital calculations; performance characteristics of different tetrahydrozoline sensors; simultaneous voltammetric determination of tetrahydrozoline and chloramphenicol; and penalty points (PPs) for the differential pulse voltammetric determination of tetrahydrozoline at the copper oxide/zeolite nanostructure and gold-plated carbon paste electrode (PDF)

■ AUTHOR INFORMATION

Corresponding Author

Nashwa M. El-Metwaly − *Department of Chemistry, College of Sciences, Umm Al-Qura University, Makkah 24230, Saudi Arabia; Department of Chemistry, Faculty of Science, Mansoura University, Mansoura 002050, Egypt;* orcid.org/0000-0002-0619-6206; Email: n_elmetwaly00@yahoo.com

Authors

Hana M. Abumelha − *Department of Chemistry, College of Science, Princess Nourah bint Abdulrahman University, Riyadh 11671, Saudi Arabia*

Ali Sayqal − *Department of Chemistry, College of Sciences, Umm Al-Qura University, Makkah 24230, Saudi Arabia*

Razan M. Snari − *Department of Chemistry, College of Sciences, Umm Al-Qura University, Makkah 24230, Saudi Arabia*

Kholood M. Alkhamis − *Department of Chemistry, Faculty of Science, University of Tabouk, Tabouk 71421, Saudi Arabia*

Arwa Alharbi − *Department of Chemistry, College of Sciences, Umm Al-Qura University, Makkah 24230, Saudi Arabia*

Zehbah A. Al-Ahmed − *Applied College Dhahran Aljanoub, King Khalid University, Abha 61421, Saudi Arabia*

Complete contact information is available at: https://pubs.acs.org/10.1021/acsomega.4c00370

Notes

The authors declare no competing financial interest.

Not applicable

Not applicable

■ ACKNOWLEDGMENTS

This study was suppoerted by the Princess Nourah bint Abdulrahman University Researchers Supporting Project number (PNURSP2024R22) and Princess Nourah bint Abdulrahman University, Riyadh, Saudi Arabia.

■ REFERENCES

(1) Sweetman, S. C.; Martindale, C. . *The complete drug reference*. 35th edn; Pharmaceutical Press, 2005.

(2) B. P. Commission. *British Pharmacopoeia, British Pharmacopoeia Commission*; HM Stationery Office: London, TSO, UK, 2013.

(3) Stillwell, M. E.; Saady, J. J. Use of tetrahydrozoline for chemical submission. *Forensic science international* **2012**, *221*, e12−e16.

(4) Hosten, L. O.; Snyder, C. Over-the-Counter Ocular Decongestants in the United States−Mechanisms of Action and Clinical Utility for Management of Ocular Redness. *Clin. Optom.* **2020**, 95−105.

(5) Daggy, A.; Kaplan, R.; Roberge, R.; Akhtar, J. Pediatric VISINE (tetrahydrozoline) ingestion: case report and review of imidazoline toxicity. *Vet. Hum. Toxicol.* **2003**, *45* (4), 210−212.

(6) Spiller, H.; Griffith, J. Prolonged cardiovascular effects after unintentional ingestion of tetrahydrozoline. *Clinical toxicology* **2008**, *46* (2), 171−172.

(7) Jensen, P. A. U. L.; Edgren, B.R.U.C.E.; Hall, L. O. I. S.; Ring, J. C. Hemodynamic effects following ingestion of an imidazoline-containing product. *Pediatric emergency care* **1989**, *5* (2), 110−112.

(8) Tobias, J. D. Central nervous system depression following accidental ingestion of VISINE eye drops. *Clinical pediatrics* **1996**, *35* (10), 539−540.

(9) Osterhoudt, K. C.; Henretig, F. M. Sinoatrial node arrest following tetrahydrozoline ingestion. *Journal of Emergency Medicine* **2004**, *27* (3), 313−314.

(10) Lowry, J. A.; Garg, U. Serum concentrations in three children with unintentional tetrahydrozoline overdose. *Clinical toxicology* **2011**, *49* (5), 434−435.

(11) Lev, R.; Clark, R. F. VISINE® overdose: Case report of an adult with hemodynamic compromise. *Journal of emergency medicine* **1995**, *13* (5), 649−652.

(12) Holmes, J. F.; BERMAN, D. A. Use of naloxone to reverse symptomatic tetrahydrozoline overdose in a child. *Pediatric emergency care* **1999**, *15* (3), 193−194.

(13) Menshawey, E.; Menshawey, R. More than meets the eye: a scoping review on the non-medical uses of THZ eye drops. *Forensic Sci., Med., Pathol.* **2023**, 1−10.

(14) Spiller, H. A.; Siewert, D. J. Drug-Facilitated Sexual Assault Using Tetrahydrozoline. *Journal of forensic sciences* **2012**, *57* (3), 835−838.

(15) Spiller, H. A.; Rogers, J.; Sawyer, T. S. Drug facilitated sexual assault using an over-the-counter ocular solution containing tetrahydrozoline (VISINE®). *Legal medicine* **2007**, *9* (4), 192−195.

(16) Carr, M. E.; Engebretsen, K. M.; Ho, B.; Anderson, C. P. Tetrahydrozoline (VISINE®) concentrations in serum and urine during therapeutic ocular dosing: a necessary first step in determining an overdose. *Clinical Toxicology* **2011**, *49* (9), 810−814.

(17) United States Pharmacopeia *National Formulary 26*, vol.*31*, Rockville, MD, 2011; p.3316.

(18) *British Pharmacopeia*, London, UK, 2010; p.348.

(19) Altuntas, T. G.; Korkmaz, F.; Nebioglu, D. Determination of tetrahydrozoline hydrochloride and fluorometholone in pharmaceutical formulations by HPLC and derivative UV spectrophotometry. *Die Pharmazie* **2000**, *55* (1), 49−52.

(20) Ali, M. S.; Ghori, M.; Saeed, A. Simultaneous determination of ofloxacin, tetrahydrozoline hydrochloride, and prednisolone acetate

by high-performance liquid chromatography. *Journal of chromatographic science* **2002**, *40* (8), 429−433.
(21) Huang, M. C.; Ho, H. O.; Wen, K. C.; Sheu, M. T. High performance liquid chromatography analysis of tetrahydrozoline hydrochloride in ophthalmic solution by silica column eluted with aqueous solvent mixtures. *J, Food Drug Anal.* **2002**, *10* (2), 88−94.
(22) Al-Rimawi, F.; Zareer, W.; Rabie, S.; Quod, M. Development and validation of a reversed-phase HPLC method for analysis of tetrahydrozoline hydrochloride in eye drop formulations. *Journal of pharmaceutical analysis* **2012**, *2* (1), 67−70.
(23) El-Bagary, R. I.; Fouad, M. A.; El-Shal, M. A.; Tolba, E. H. Stability-indicating RP-HPLC methods for the determination of fluorometholone in its mixtures with sodium cromoglycate and tetrahydrozoline hydrochloride. *Journal of chromatographic science* **2016**, *54* (6), 923−933.
(24) Hymete, A. B. A.; Bekhit, A. A. Development and validation of HPTLC densitometric method for simultaneous determination of antazoline hydrochloride and tetryzoline hydrochloride in eye drop and its application as stability indicator. *Thai J. Pharm. Sci.* **2013**, *37* (3), 134−145.
(25) Gumustas, M.; Alshana, U.; Ertas, N.; Goger, N. G.; Ozkan, S. A.; Uslu, B. Determination of antazoline and tetrahydrozoline in ophthalmic solutions by capillary electrophoresis and stability-indicating HPLC methods. *J. Pharm. Biomed. Anal.* **2016**, *124*, 390−398.
(26) Salem, H.; Lotfy, H. M.; Hassan, N. Y.; El-Zeiny, M. B.; Saleh, S. S. A comparative study of different aspects of manipulating ratio spectra applied for ternary mixtures: derivative spectrophotometry versus wavelet transform. *Spectrochimica Acta Part A: Molecular and Biomolecular Spectroscopy* **2015**, *135*, 1002−1010.
(27) Lotfy, H. M.; Saleh, S. S.; Hassan, N. Y.; Salem, H. A comparative study of novel spectrophotometric methods based on isosbestic points; application on a pharmaceutical ternary mixture. *Spectrochimica Acta Part A: Molecular and Biomolecular Spectroscopy* **2014**, *126*, 112−121.
(28) Lotfy, H. M.; Saleh, S. S.; Hassan, N. Y.; Salem, H. Novel two wavelength spectrophotometric methods for simultaneous determination of binary mixtures with severely overlapping spectra. *Spectrochimica Acta Part A: Molecular and Biomolecular Spectroscopy* **2015**, *136*, 1786−1796.
(29) Mohamed, G. G.; Rizk, M. S.; Frag, E. Y. Z. spectrophotometric determination of distigmine bromide, cyclopentolate HCl, diaveridine HCl and tetrahydrozoline HCl via charge transfer complex formation with TCNQ and TCNE reagents. *Iran. J. Pharm. Res.* **2015**, *14* (3), 701.
(30) Siddiqui, M. R.; AlOthman, Z. A.; Rahman, N. Analytical techniques in pharmaceutical analysis: A review. *Arab. J. Chem.* **2017**, *10*, S1409−S1421.
(31) Ozkan, S. A. *Electroanalytical methods in pharmaceutical analysis and their validation*. HNB publishing,, 2012. Ozkan, S. A.; Kauffmann, J. M.; Zuman, P. *Electroanalysis in biomedical and pharmaceutical sciences: voltammetry, amperometry, biosensors, applications*. Springer, 2015.
(32) Ziyatdinova, G.; Budnikov, H. Electroanalysis of antioxidants in pharmaceutical dosage forms: state-of-the-art and perspectives. *Monatshefte Chem. Chem. Monthly* **2015**, *146*, 741−753.
(33) Kurbanoglu, S.; Ozkan, S. A.; Merkoçi, A. Electrochemical Nanobiosensors in Pharmaceutical Analysis. *Novel Developments Pharm. Biomed. Anal.* **2018**, *2*, 302−353.
(34) Hassan, N. Y.; Lotfy, H. M.; Saleh, S. S.; Salem, H. Development of membrane electrodes for the specific determination of tetryzoline hydrochloride in presence of its degradation product in pharmaceutical formulations and biological fluids. *Anal. Bioanal. Electrochem.* **2015**, *2015*, 7.
(35) Mahmoud, A. M.; Saad, M. N.; Elzanfaly, E. S.; Amer, S. M.; Essam, H. M. An electrochemical sensing platform to determine tetrahydrozoline HCl in pure form, pharmaceutical formulation, and rabbit aqueous humor. *Analytical Methods* **2020**, *12* (22), 2903−2913.
(36) Habib, A. A.; Hendawy, H. A.; Hammad, S. F.; Bebawy, L. I.; Girges, M. A. Electrochemical Approach for Determination of Tertahydrozoline HCl using Gold Nanoparticles Electrode. *Anal. Bioanal. Electrochem.* **2020**, *12* (2), 223.
(37) Bounegru, A. V.; Apetrei, C. Carbonaceous nanomaterials employed in the development of electrochemical sensors based on screen-printing technique—A review. *Catalysts* **2020**, *10* (6), 680.
(38) Kamarudin, S. F.; Mustapha, M.; Kim, J. K. Green strategies to printed sensors for healthcare applications. *Polym. Rev.* **2021**, *61* (1), 116−156.
(39) Maddipatla, D.; Narakathu, B. B.; Atashbar, M. Recent progress in manufacturing techniques of printed and flexible sensors: a review. *Biosensors* **2020**, *10* (12), 199.
(40) Ferrari, A. G. M.; Rowley-Neale, S. J.; Banks, C. E. Screen-printed electrodes: Transitioning the laboratory in-to-the field. *Talanta Open* **2021**, *3*, No. 100032.
(41) Ambaye, A. D.; Kefeni, K. K.; Mishra, S. B.; Nxumalo, E. N.; Ntsendwana, B. Recent developments in nanotechnology-based printing electrode systems for electrochemical sensors. *Talanta* **2021**, *225*, No. 121951.
(42) Qian, L.; Durairaj, S.; Prins, S.; Chen, A. Nanomaterial-based electrochemical sensors and biosensors for the detection of pharmaceutical compounds. *Biosen. Bioelectron.* **2021**, *175*, No. 112836.
(43) Agnihotri, A. S.; Varghese, A.; Nidhin, M. Transition metal oxides in electrochemical and bio sensing: A state-of-art review. *Appl. Sur. Sci. Adv.* **2021**, *4*, No. 100072.
(44) Bozal-Palabiyik, B.; Erkmen, C.; Kurbanoglu, S.; Ozkan, S. A.; Uslu, B. Electrochemical analysis for pharmaceuticals by the advantages of metal oxide nanomaterials. *Current Analytical Chemistry* **2021**, *17* (9), 1322−1339.
(45) Maciulis, V.; Ramanaviciene, A.; Plikusiene, I. Recent Advances in Synthesis and Application of Metal Oxide nanostructures in Chemical Sensors and Biosensors. *Nanomaterials* **2022**, *12*, 4413.
(46) Falola, T. O. Nanoparticles Modified Electrodes: Synthesis, Modification, and Characterization—A Review. *World Journal of Nano Science and Engineering* **2022**, *12* (3), 29−62.
(47) Habibi, B.; Pashazadeh, S.; Pashazadeh, A.; Saghatforoush, L. A. An amplified electrochemical sensor employing one-step synthesized nickel−copper−zinc ferrite/carboxymethyl cellulose/graphene oxide nanosheets composite for sensitive analysis of omeprazole. *RSC Adv.* **2023**, *13* (43), 29931−29943.
(48) Xiao, J.; Wang, H.; Li, C.; Deng, K.; Li, X. A simple dopamine sensor using graphdiyne nanotubes and shortened carbon nanotubes for enhanced preconcentration and electron transfer. *Microchemical Journal* **2021**, *160*, No. 105755.
(49) Liu, X.; Deng, K.; Wang, H.; Li, C.; Zhang, S.; Huang, H. Aptamer based ratiometric electrochemical sensing of 17β-estradiol using an electrode modified with gold nanoparticles, thionine, and multiwalled carbon nanotubes. *Microchim. Acta* **2019**, *186*, 1−8.
(50) Sannegowda, L. K.; Reddy, K. V.; Shivaprasad, K. H. Stable nano-sized copper and its oxide particles using cobalt tetraamino phthalocyanine as a stabilizer; application to electrochemical activity. *RSC Adv.* **2014**, *4* (22), 11367−11374.
(51) Nemakal, M.; Palanna, M.; Sannegowda, L. K.; Kumar, P. S. Zinc phthalocyanine anchored magnetite particles: Efficient platform for sensing of thiocyanate. *J. Electroanal. Chem.* **2021**, *895*, No. 115385.
(52) Hendawy, H. A.; Khaled, E.; Radowan, A. voltammetric determination of Marbofloxacin at carbon paste sensor integrated with copper oxide nanoparticles. *Electroanalysis* **2023**, *35* (5), No. e202200402.
(53) Al-Bonayan, A. M.; Hameed, A.; Alorabi, A. Q.; Alessa, H.; Aljuhani, E.; El-Metwaly, N. M. Novel Copper Oxide Nanostructure Propafenone voltammetric Sensor. *Arabian J. Sci. Eng.* **2023**, 1−10.
(54) Aldawsari, A. M.; Khalifa, M. E.; Munshi, A. M.; Shah, R.; Keshk, A. A.; Saad, F.; El-Metwaly, N. M. Copper oxide based disposable sensors for sensitive voltammetric assay of Sumatriptan. *Int. J. Electrochem. Sci.* **2021**, *16* (5), No. 210540.

https://doi.org/10.1021/acsomega.4c00370
ACS Omega 2024, 9, 13458−13468

(55) Al-Bonayan, A. M.; Althakafy, J. T.; Alorabi, A. Q.; Alamrani, N. A.; Aljuhani, E. H.; Alaysuy, O.; Al-Qahtani, S. D.; El-Metwaly, N. M. Novel Copper Oxide-Integrated Carbon Paste Tirofiban voltammetric Sensor. *ACS omega* **2023**, *8* (5), 5042−5049.
(56) Al-Qahtani, S. D.; Al-nami, S. Y. Copper oxide nanopowder modified carbon paste electrode for the voltammetric assay of vonoprazan. *Arabian Journal of Chemistry* **2021**, *14* (8), No. 103254.
(57) Ahmadpour-Mobarakeh, L.; Nezamzadeh-Ejhieh, A. A zeolite modified carbon paste electrode as useful sensor for voltammetric determination of acetaminophen. *Materials Science and Engineering: C* **2015**, *49*, 493−499.
(58) Amare, M. voltammetric determination of paracetamol in tablet formulation using Fe(III) doped zeolite-graphite composite modified GCE. *Heliyon* **2019**, *5*, No. e01663.
(59) Al-Qahtani, S. D.; Hameed, A.; Aljuhani, E.; Sayqal, A.; Shah, R.; Saad, F.; El-Metwaly, N. M. Novel Zeolite Modified Carbon Paste Electrode for Differential Pulse voltammetric Assay of Cyclopentolate hydrochloride. *Int. J. Electrochem. Sci.* **2021**, *16* (6), No. 210628.
(60) Al-Nami, S. Y.; Hameed, A.; Azher, O. A.; Alamrani, N. A.; Aljuhani, E.; Abumelha, H. M.; El-Metwaly, N. M. Integrated Zeolite Based Carbon Paste Electrode for Sensitive voltammetric Assay of Ticagrelor. *Arabian Journal for Science and Engineering* **2023**, *48* (1), 539−549.
(61) Snari, R. M.; Alharbi, A.; Munshi, A.; Al-Ahmed, Z. A.; Aljuhani, E.; Alluhaybi, A. A.; Althagafi, I.; Elmetwaly, N. Zirconium Oxide Nanostructure Integrated Screen-Printed Mirabegron voltammetric Sensors. *J. Electrochem. Soc.* **2023**, DOI: 10.1149/1945-7111/ad0d1a.
(62) Jouikov, V.; Simonet, J. Electrochemical reactions of sulfur organic compounds. *Encycl. Electrochem.* **2007**, DOI: 10.1002/9783527610426.bard080009.
(63) Heli, H.; Zarghan, M.; Jabbari, A.; Parsaei, A.; Moosavi-Movahedi, A. A. Electrocatalytic oxidation of the antiviral drug acyclovir on a copper nanoparticles-modified carbon paste electrode. *J. Solid State Electrochem.* **2010**, *14*, 787−795.
(64) Stanković, D.; Mehmeti, E.; Svorc, L.; Kalcher, K. New electrochemical method for the determination of β-carboline alkaloids, harmalol and harmine, in human urine samples and in Banisteriopsis caapi. *Microchem. J.* **2015**, *118*, 95−100.
(65) Wu, A. B.; Huang, M. C.; Ho, H. O.; Yeh, G. C.; Sheu, M. T. Investigation on liquid chromatographic separation of basic compounds using silica column with aqueous/organic mobile phase containing triethylamine and acetic acid. *Biomedical Chromatography* **2004**, *18* (7), 443−449.
(66) Zhang, Z.; Wang, E. *Electrochemical principles and methods*; Science Press: Beijing, 2000.
(67) Gosser, D. K. *Cyclic voltammetry, simulation and analysis of reaction mechanisms*; Wiley VCH: New York, 1993.
(68) Elgrishi, N.; Rountree, K. J.; McCarthy, B. D.; Rountree, E. S.; Eisenhart, T. T.; Dempsey, J. L. A practical beginner's guide to cyclic voltammetry. *J. Chem. Educ.* **2018**, *95*, 197−206.
(69) Laviron, E. Theoretical study of a reversible reaction followed by a chemical reaction in thin layer linear potential sweep voltammetry. *J. Electroanal. Chem. Interfacial Electrochem.* **1972**, *39*, 1.
(70) Bard, A. J.; Faulkner, L. R. *Electrochemical Methods Fundamentals and Applications*, 2nd ed., Wiely: New York, 2004.
(71) Ngamchuea, K.; Eloul, S.; Tschulik, K.; Compton, R. G. Planar diffusion to macro disc electrodes—what electrode size is required for the Cottrell and Randles-Sevcik equations to apply quantitatively? *J. Solid State Electrochem.* **2014**, *18*, 3251−3257.
(72) Currie, L. A. International recommendations offered on analytical detection and quantification concepts and nomenclature. *Anal. Chim. Acta* **1999**, *391*, 103−134.
(73) *International Conference on Harmonisation of Technical Requirements for the Registration of Pharmaceuticals for Human Use (ICH) guideline Q3A(R2), Impurities in new drug substances*, 2006.
(74) Ahuja, S. *Impurities evaluation of pharmaceuticals*; Marcel Dekker: New York, (1998).
(75) Bauer, J.; Krogh, S. High-performance liquid chromatographic stability-indicating assay for naphazoline and tetrahydrozoline in ophthalmic preparations. *Journal of pharmaceutical sciences* **1983**, *72* (11), 1347−1349.
(76) Lotfy, H. M.; Saleh, S. S.; Hassan, N. Y.; Salem, H. Development and validation of impurity-profiling UPLC method for the determination of sodium cromoglicate and tetryzoline hydrochloride: Application on rabbit aqueous humor. *Journal of Chromatography B* **2015**, *1006*, 121−129.
(77) Gałuszka, A.; Migaszewski, Z. M.; Konieczka, P.; Namieśnik, J. Analytical Eco-Scale for assessing the greenness of analytical procedures. *TrAC Trends in Analytical Chemistry* **2012**, *37*, 61−72.
(78) Tobiszewski, M.; Marć, M.; Gałuszka, A.; Namieśnik, J. Green chemistry metrics with special reference to green analytical chemistry. *Molecules* **2015**, *20* (6), 10928−10946.
(79) Serrano-Luján, L.; Víctor-Román, S.; Toledo, C.; Sanahuja-Parejo, O.; Mansour, A. E.; Abad, J.; Amassian, A.; Benito, A. M.; Maser, W. K.; Urbina, A. Environmental impact of the production of graphene oxide and reduced graphene oxide. *SN Appl. Sci.* **2019**, *1* (2), 1−12.

https://doi.org/10.1021/acsomega.4c00370
ACS Omega 2024, 9, 13458−13468